Composites: Part A 43 (2012) 310–316

Contents lists available at SciVerse ScienceDirect

Composites: Part A

journal homepage: www.elsevier.com/locate/compositesa

Full-field analysis of shear test on 3D orthogonal woven C/C composites

Lijun Qin [a], Zhongwei Zhang [b], Xiaofeng Li [a], Xiaoguang Yang [b], Zhihai Feng [b], Yang Wang [a], Hong Miao [a], Linghui He [a], Xinglong Gong [a,*]

[a] CAS Key Laboratory of Mechanical Behavior and Design of Materials, Department of Modern Mechanics, University of Science and Technology of China, Hefei 230027, China
[b] Aerospace Research Institute of Material and Processing Technology, Beijing 100076, China

ARTICLE INFO

Article history:
Received 28 September 2011
Received in revised form 10 November 2011
Accepted 11 November 2011
Available online 20 November 2011

Keywords:
A. 3-Dimensional reinforcement
B. Mechanical properties
D. Mechanical testing
Full-field measurements

ABSTRACT

In this work, the digital image correlation (DIC) technique was used as full-field measurement to analyze the shear properties of the 3D orthogonal woven C/C composites. Both the in-plane and the through-the-thickness specimens were tested and the macroscopic average strain was obtained. The composites were composed of lots of periodic units and the macroscopic average strain was dependent on these meso-structures. There were three regions within one unit, which showed different mesoscopic strain. The relationship between the shear test region and the macroscopic average strain was systematically studied. Finally, the accuracy of conventional strain-gauge rosette measurement was also discussed.

1. Introduction

Three-dimensional (3D) carbon/carbon (C/C) composites have attracted considerable attention and been widely used in aviation, aerospace and naval industry [1,2]. Due to their 3D architecture, the C/C composites show lots of merits such as strong through-the-thickness properties, high damage tolerance, and dimensional stability [2–5]. For the purpose of materials selection decision and structure designing, correct determination of mechanical properties is still a very essential and also actual issue. Among the mechanical static tests, the shear properties is the most difficult type to be acquired [6]. Thus, the determination of shear modulus for 3D woven composites should be more sophisticated and challengeable because of their structure heterogeneity.

Several methods such as thin-walled tube torsion test [7], rail shear test [8–10], off-axis shear test [11–13], and Iosipescu shear test [14–16] have been developed to measure shear properties of composites. However, all of them are originally used for homogeneous materials. The 3D C/C composites which are composed of lots of periodic units are heterogeneous. The size of the units can reach to as large as 2–10 mm and the deformation field may be highly inhomogeneous on this mesoscale level [17]. Since the mesoscale of the homogeneous materials is quite small in comparison to the specimens' dimension, the mesoscopic strain of the homogeneous materials can be ignored. However, it contributes a lot to the macroscopic strain in the heterogeneous one. The shear elastic property is a macroscopic mechanical characteristic, which is usually used to evaluate the structural performance. During the shear testing, if the test section of the specimen is on the relative stiffness part of the unit, the strain will be much larger than that of the soft part. The accurate determination of the shear modulus directly depends on correct selection of the representative macroscopic average strain. In this case, both the meso-field and macro-field shear deformation are important to the material testing. The influence of the material heterogeneity on the macro-field average strain is requisite for the accurate determination of the shear modulus.

A full-field measurement can be employed to fully understand the shear property of the heterogeneous materials. Since 1990s, moiré interferometry was developed as a chief full-field technique in woven composites measurements. Ho and his colleagues [18] have done many pioneer works in this area and tested the shear properties of graphite–woven composites by using moiré interferometry as the full field technique. The distributions of the shear strain for the specimen were studied and the extremely inhomogeneous strain was firstly investigated. Additionally, based on the moiré interferometry, several important works were also done for tensile and compression test of the woven composites [19–22]. However, an interferometric laser is prerequisite in this method. The laser needs complex optical setup and it is very sensitive to the vibration. In addition, the specimen should be prepared by density diffraction gratings and these processes are complex and costly. These drawbacks highly limited their practical application, thus new full-field technique should be introduced for testing the 3D C/C composites.

* Corresponding author. Fax: +86 551 3600419.
E-mail address: gongxl@ustc.edu.cn (X. Gong).

1359-835X/$ - see front matter © 2011 Elsevier Ltd. All rights reserved.
doi:10.1016/j.compositesa.2011.11.006

Recently, full-field measurement digital image correlation (DIC) technique has attracted tremendous research interests owing to its various advantages, such as white light illumination, no sensitivity to the vibration, relative simplicity of the sample preparation and sufficient accuracy of the measurements. It is becoming the main full-field technique in many fields of solid mechanics, include determination of stress–strain response [23–26], observation fracture and crack grow [27–30], stress intensity [28,31,32], investigation high temperature [33–35] and high strain [36] mechanical properties, and residual stress [37,38]. Due to its excellent effectiveness and convenience, DIC technique has been increasingly applied to measure the displacements and strains of the 2D and 3D architecture composite materials. During the past decades, the DIC method has been applied to study the mechanical properties of the twill-weave composite [39,40], carbon–epoxy triaxial–braided [41], and 3D woven C/SiC composite [42]. The correct determination of mesoscopic deformation of many heterogeneous composite materials can be successfully achieved by using this method. However, the influence of materials structure heterogeneity on the macroscopic average shear strain has not been carefully studied by using the DIC technique. More work should be done to accurately measure the shear modulus of 3D composites and systematically investigate their structural dependent mechanical properties.

In this work, DIC technique was used as a full-field measurement to analyze the shear test of the 3D orthogonal woven C/C composites. Both the in-plane and the through-the-thickness specimens were tested. Different strain regions within one unit cell and the macroscopic strain distribution on test section were analyzed. The relationship between the shear region and the macroscopic average strain was discussed. Finally, the accuracy of conventional strain-gauge rosette measurement was also studied.

2. Materials and experiments

2.1. Material and specimens

3D orthogonal woven carbon/carbon composite is studied in this work and its architecture is shown in Fig. 1. Define the fiber bundles in direction 1, 2 and 3 as 1-yarns, 2-yarns and 3-yarns, respectively. The fiber bundles in three material directions are mutually orthogonal. It is fabricated by Liquid Phase Infiltration process and the fiber bundles are carbon fiber T300. Firstly, the 1-yarns and 2-yarns are orthogonally laid one-by-one ply. Then, the 3-yarns fill the 1- and 2- yarns plane in through-the-thickness direction. At last, the 3D orthogonal architectures are filled by the pitch and carbonized in high-temperature. The unit cell dimension in-plane is approximately 2.4 mm and ply thickness is about 0.25 mm. In order to characterize the strain distribution within one unit structure cell, the unit cell was divided by three regions, as shown in Fig. 1, region-1 is made up of two direction fiber bundles (1-yarns and 2-yarns), region-2 is made up of one direction fiber bundles (1-yarns or 2-yarns) and matrix, and region-3 consists of one direction fiber bundles (3-yarns) only.

The Iosipescu shear test is applied following the ASTM D 5379 norm. As shown in Fig. 2, the specimen is 76 mm long and 20 mm wide with two V-notches on the opposite ends of the vertical center line. The test section length between two notches is 12 mm, the depth of the notches is 4 mm, the notch angle is 90°, and the notches are rounded at the tips with a radius $R = 1.5$ mm. The specimens are cut from both plane 1-2 and plane 1-3(or 2-3).

2.2. Full field measurement technique

DIC is an optical, full field displacement measurement technique. It can obtain the full field relative displacements from two digital images which have embodied the deformational information of the specimen. Fig. 3 shows the basic principle of DIC. The reference image I1 records the object surface feature before deformation, and I2 records the one after deformation. For example, a point $\mathbf{p}$ (position vector $\mathbf{r}$) and its adjacent area S1 (called subimage) is in the I1. After deformation, they change to the point $\mathbf{p}'$ (position vector $\mathbf{r}'$) and subimage S2 in the I2. Here, the DIC method is used to detect the location of $\mathbf{p}'$ reliably and accurately. If the position $\mathbf{r}'$ in the deformed image is determined, the displacement vector $\mathbf{d}$ can be determined: $\mathbf{d} = \mathbf{r}' - \mathbf{r}$. If the full field displacements of the surface are obtained, the deformation would be achieved.

Generally, in order to match subimages uniquely and accurately, the object surface must have random speckle pattern which deforms together with the object. The speckle pattern can be natural feature of object or artificial feature. In this study, the surfaces of specimens are prepared by spraying the black and white paints. The DIC algorithm routine is used to find the true position $\mathbf{p}'$ which make the correlation function minimum. Then, the displacements fields $\mathbf{d}$ can be obtained. More details of DIC method can be found in Refs. [43–47]. The average accuracy of displacement values in present DIC algorithm is about 0.01 pixel.

After displacements fields $\mathbf{d}$ are estimated, in-plane strain fields can be calculated by numerical difference method. In order to increase strain spatial resolution, small subimage and step size should be taken. However, when the subimage is too small, the error of estimated displacements will be large. Thus an optimal subimage size is needed. If the step size is too small, the strain error made by numerical differentiating process will be very huge even noise of displacement field is small. In order to eliminate this error, a data smoothing technique is requested. A local quadratic fitting smoothing method is used to smooth the displacements field and obtain the more accurate strain fields. In this study, the subimage size is taken 37×37 ($\sim 41 \times 41$) pixels, the step size is 5×5 pixels. The smoothing window is 9×9.

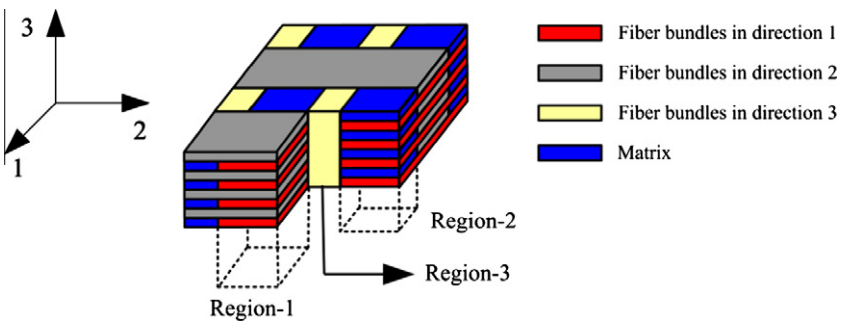

Fig. 1. Architecture model of 3D woven C/C composite. (For interpretation of the references to color in this figure legend, the reader is referred to the web version of this article.)

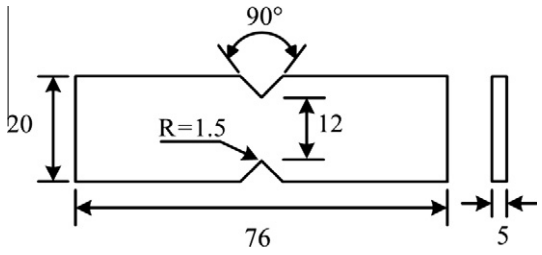

Fig. 2. Iosipescu shear test specimen (dimensions in mm).

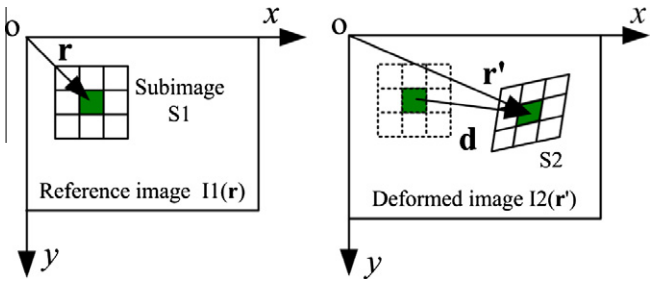

Fig. 3. Schematic showing the principle of DIC. (For interpretation of the references to color in this figure legend, the reader is referred to the web version of this article.)

2.3. Experiments details

The Iosipescu shear test is widely used to test shear properties of woven composites [48–53]. During the experiment, two counteracting force couples are applied to a specimen and a state of constant shear force is induced in the mid-plane of the specimen. Induced moments cancel each other out at the midsection thereby producing a state of pure shear in the region between the two notches [54]. The test fixture (Fig. 4) is fabricated in-house machinery plant according the modified Wyoming version. Fig. 4 shows the shear test setup, the fixture mounted in the material test machine MTS 809 and the optical system is also setup. The quasi-static load speed is 0.05 mm/min and the images sampling rate is 30 pictures per min. It is reported that the strains on the front of specimens are difficult to coincide with values on the back due to the undesirable twist and average of two surface values is needed [55,56]. To eliminate these differences between the two surfaces, two optical setups are established both from the front and back of the shear texture (Fig. 4). Two CCD captured the images from both surfaces of specimen simultaneously during the whole loading process and the two sequences of the images are continuously read into the one computer. The resolution of the CCD camera is 1280×960 pixels and the specimen is illuminated by the white light source. Telecentric lens used here are expected to overcome disadvantages of the traditional lens. For traditional lens, two aspects will introduce a relatively high strain error, one is the lens magnification variation due to the small out-of-plane displacement of specimen, and the other is the lens distortion [57]. By using the telecentric lens, these two problems can be solved perfectly.

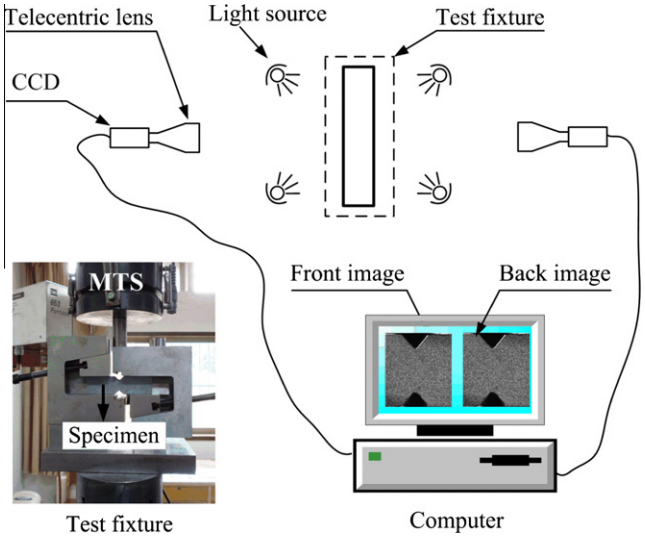

Fig. 4. Optical Iosipescu shear test system setup. (For interpretation of the references to color in this figure legend, the reader is referred to the web version of this article.)

3. Results and discussion

3.1. Full field strain distribution and analysis

Fig. 5a shows the reference speckle image before applying the shear loading. By comparing the deformed image and the reference image, the shear strain can be obtained by DIC (Fig. 5b). As shown in strain contour, the strain is nonuniform and they are periodically distributed in the test region. The tested materials show a typical periodic structure and the strains period agree well with the material unit cell. The magnitude of strain depends on the material fiber architecture. As shown in Fig. 6, the strain contour indicates that the strain is the highest in the region-1, smaller in the region-2, and smallest in the region-3. The strain ratio of region-1, -2 and -3 can reach to 1:1.6:4. This conclusion is summarized from Fig. 5 and Fig. 10, where the region-2,-3 and region-1,-2 are on the same stress condition. As shown in Fig. 1, region-3 consisted through-the-thickness fiber bundles (3-yarns) only. When the shear is loaded in-plane, the shear resistance is the weakest, thus the relative strain is the largest. Region-1 is made up of two direction fiber bundles (1-yarns and 2-yarns), its in-plane shear resistance is the strongest, and thus its strain is the smallest. The region-2 is made up of one direction fiber bundles and matrix, which makes it in the middle of the region-1 and -3. In order to explain the relationship between the fluctuant shear strain and the material architecture, the fiber bundles architecture after loading is shown in Fig. 5c. Although extensive damage is visible, the different regions are still easy to be distinguished out. It should be noted that the DIC method is difficult to give accurate values after the occurring of visible fracture. Thus, DIC measurements are interrupted before significant damage occurred.

The normalization shear strain along the notches in Fig. 7 illustrates the strain non-uniformity evolution when the shear loading increases. With increasing of the stress, the local strain increases accordingly. However, the highest and lowest strain locations are almost kept the same. The strain distribution is unchangeable and the strain ratios on different region of the unit cell are invariant. It can be observed that the bias between local strain and average strain may be 50%. From this result one can conclude that test zone, on which the average strain defined as specimen macroscopic strain is used to determine the shear modulus, must be large enough so as the average strain can damp the oscillation caused by the local large and low strain. Fig. 8 shows the average strain at different distance along the two notches. It is found that the amplitude of the oscillation is damping while the distance increases. It should be noted that the local larger strain can be offset by the local lower strain on one strain period, thus the average strain on the distance at half period unit cell length may have a largest bias.

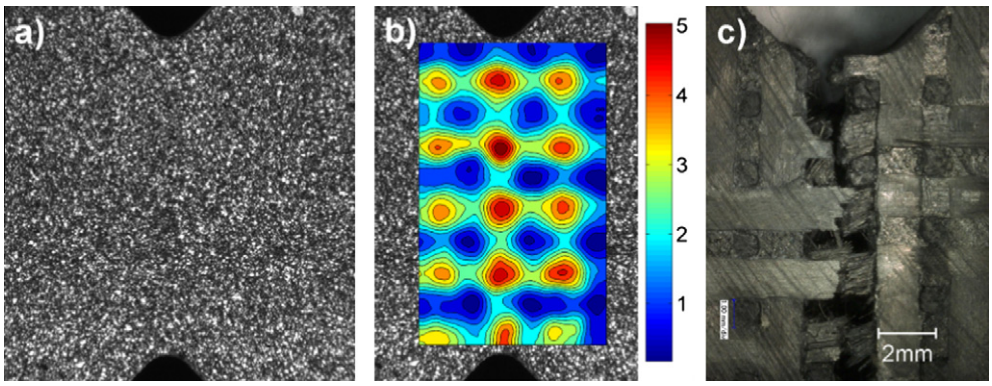

Fig. 5. In-plane specimen 1#: (a) initial image (reference image); (b) shear strain contour (1000 με) at 12.3 MPa and (c) fiber bundles architecture. (For interpretation of the references to color in this figure legend, the reader is referred to the web version of this article.)

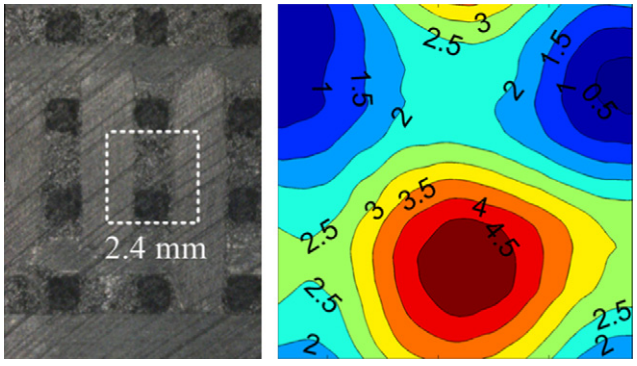

Fig. 6. Shear strain distribution on one unit cell (1000 με). (For interpretation of the references to color in this figure legend, the reader is referred to the web version of this article.)

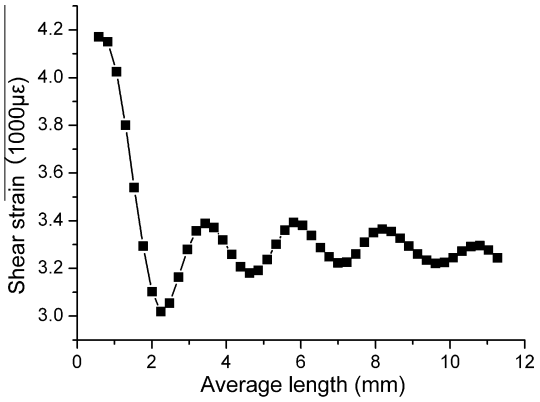

Fig. 8. Average shear strain vary with distance from bottom to upper notches.

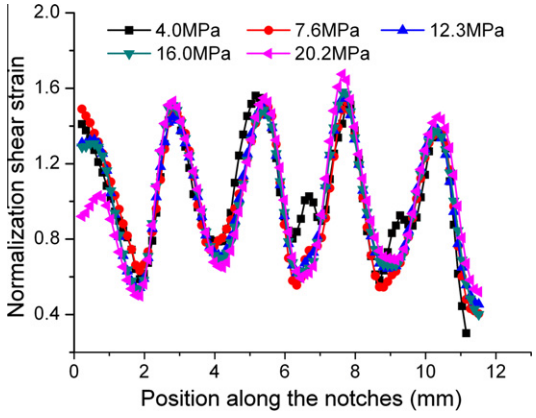

Fig. 7. Shear strain distribution along the notches at different loading. (For interpretation of the references to color in this figure legend, the reader is referred to the web version of this article.)

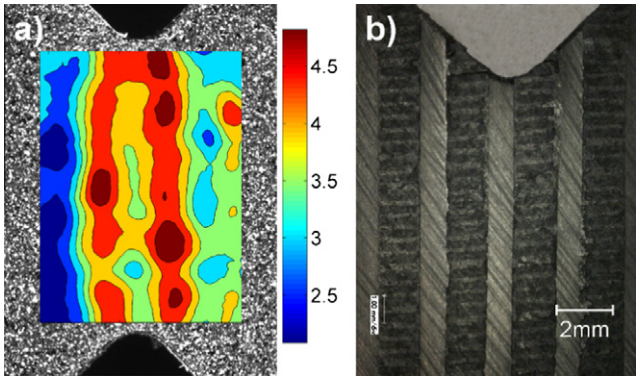

Fig. 9. Through-the-thickness specimen: (a) shear strain contour (1000 με) at 6.6 MPa and (b) fiber bundles architecture. (For interpretation of the references to color in this figure legend, the reader is referred to the web version of this article.)

Based on this study, it may be a better choice that the specimen dimensions vary with the unit cell length (UCL) scale. It should make test section contain integer multiple of UCL.

Fig. 9a shows the strain distribution of through-the-thickness specimen. The strain is relatively uniform on direction of the notches, but it is not uniform on the longitude direction. The reason is that the meso-scale (0.25 mm) in through-the-thickness direction is much smaller than that in longitude direction (2.4 mm). Thus, the non-uniform strain in through-the-thickness direction cannot be observed because it is beyond the limitation of special resolution of DIC. In comparison to fiber architecture (Fig. 9b) the relative lower strain appeared on 3-yarns, which is different to the in-plane testing results. The degree of the non-uniform is also not as extreme as in-plane.

3.2. Macroscopic strain depending on material architecture

As discussed in Section 3.1, the strain on the region-1 is greatly larger than other regions, so the macroscopic strain will depend on

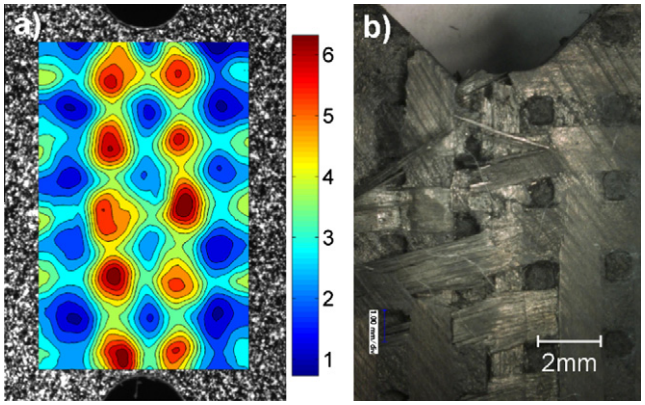

Fig. 10. In-plane specimen 2#: (a) shear strain contour (1000 με) at 12.9 MPa and (b) fiber bundles architecture. (For interpretation of the references to color in this figure legend, the reader is referred to the web version of this article.)

where the position of specimen notch is cut from the material. In order to illustrate that the macroscopic strain is highly dependent on the fiber architectures, two extreme case specimens are tested. One is the 3-yarns on the line between the two notches (specimen 1#, as shown in Fig. 5c) and the other is the 2-yarns on the line (specimen 2#, as shown in Fig. 10b). The former result is shown in Fig. 5b and the latter result is shown in Fig. 10a. Comparing the two results, it can be observed that the macroscopic strain between the notches of specimen 2# is much lower than that of specimen 1#. Thus the modulus of the specimen 2# must be higher than that of specimen 1#. Therefore, it is important to select a proper zone *A* (Fig. 12) to define the macroscopic strain, the aim of which is to meet a shear response representing the real shear deformation of materials. Ideally, the zone *A* should contain more unit cells, but the shear stress state will change if the width of zone *A* is too large. Considering the non-uniformity of the shear strain on the meso-field, one UCL should be contained in zone *A* at least. These results indicate that the specimen section should extend accordingly to the UCL scale. If the UCL is large, the specimen test section should also be large so as to guarantee the pure shear stress state on the scope of one UCL.

3.3. Strain-gauge rosette measurement simulation

Since the mesoscopic strain is extremely non-uniform, the conventional strain-gauge rosette measurement is not proper to

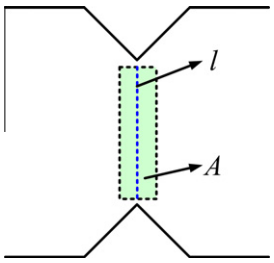

Fig. 12. Schematic diagram of calculation shear strain. (For interpretation of the references to color in this figure legend, the reader is referred to the web version of this article.)

inaccurately determine macroscopic strain. In this section, quantitative analysis is applied to illustrate how the gauge size and location affect the macro-field strain by using numerical simulation. The method is based on the foundation of strain rosette, in which the shear strain γ can be expressed by $\gamma = \varepsilon^{-45^\circ} - \varepsilon^{+45^\circ}$, where ε^{+45° and ε^{-45° is the normal strains in ±45° directions with respect to *x* axis. The gauge strain ε^{+45° and ε^{-45° can be calculated by the gauge relative displacement dividing the gauge length. The relative displacement can be calculated by projecting displacements (obtained by DIC method) on the ±45° directions with respect to *x* axis. The width of the gauge is a quarter of the length in simulation. The result is shown in Fig. 11, the *x* axis is the position of gauge center on the line between the notches, and the *y* axis is the strain-gauge result. The result confirmed that different position can make a large error and the measured value depend not only on the strain-gauge position but also the strain-gauge size. The bias at different position is sensitive to the gauge size. It can also be noted that the bias did not monotonously decrease with increasing of the gauge size. As shown in Fig. 11, the strain bias amplitude with gauge size 6/8UCL is larger than that gauge size 4/8UCL. The two extreme positions (largest strain and lowest strain) are shown in Fig. 11, where position-A represent the two gauge is on the 3-yarns and the position-B represent the center of gauge is on the 3-yarns.

3.4. Stress–strain response

The macroscopic shear stress–strain response is discussed in this section. The stress is defined by the load divided the cross-section, $\tau = \frac{P}{wt}$, where τ is the average shear stress, *P* is the applied load, *w* is the distance between the notches and *t* is the specimen thickness. There are two methods to determine the macroscopic

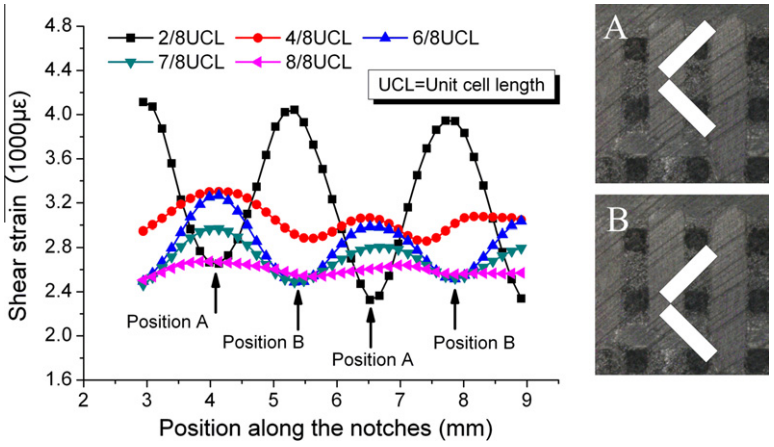

Fig. 11. Strain-gauge rosette results with different position and size. (For interpretation of the references to color in this figure legend, the reader is referred to the web version of this article.)

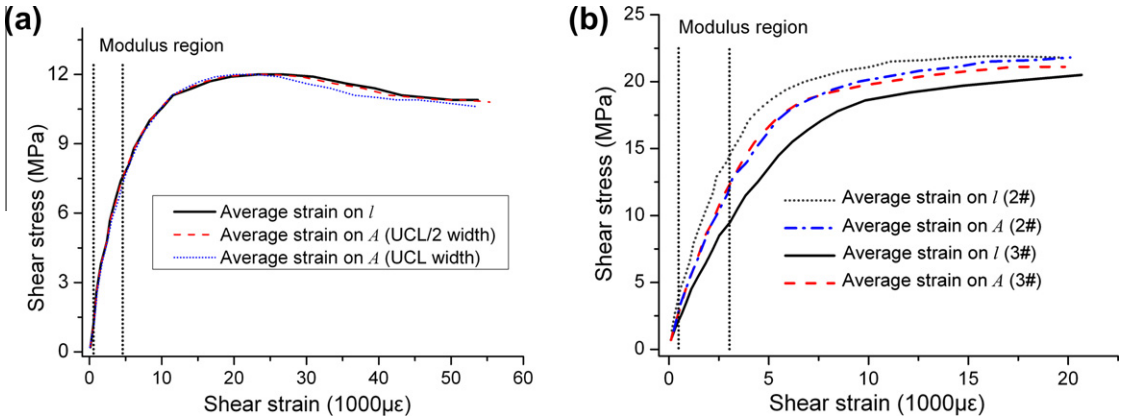

Fig. 13. Shear stress–strain curves: (a) through-the-thickness and (b) in-plane. (For interpretation of the references to color in this figure legend, the reader is referred to the web version of this article.)

shear strain (Fig. 12). One is the average shear strain along the line l, $\gamma_{avgl} = \frac{1}{l}\int_l \gamma dl$, where γ is the shear strain field determined by DIC method and the l = 9.6 mm (=4UCL). The other method is the average shear strain on the area A, $\gamma_{avgA} = \frac{1}{A}\int_A \gamma dA$, where the width of A equal 1.2 mm and 2.4 mm, representing half and one UCL.

Fig. 13 shows typical stress–strain curves, which indicates that both in-plane and through-the-thickness shear response are nonlinear. In addition, the stiffness and the strength of through-the-thickness specimens are much lower than that in the in-plan specimens. The though-the-thickness stress–strain curve is not strongly influenced by the two different strain average methods due to the relative uniform strain distribution on the specimen (as shown in Fig. 9a). However, for the in-plane specimens, this influence is great due to the dependence between macroscopic strain and the material architecture (as presented in Section 3.2). Fig. 13b shows the two typical specimens stress strain curves. Two extreme case specimens are tested. Curves 2# are the case of the 2-yarns on the notches line and curves 3# is the other extreme case of 3-yarns on the notches line. The response curves indicate that although material architecture affects the notches strain greatly, they can still converge to a stable state at one UCL width zone.

Define chord modulus as shear modulus. The strain range is from 500 to 4500 με for through-the-thickness curves. The average through-the-thickness shear modulus under different macroscopic strain are G_L = 1.58 ± 0.07 GPa, $G\_A\_0.5$ = 1.56 ± 0.11 GPa, G_A_1 = 1.51 ± 0.09 GPa, where G_L is shear modulus on the line l, $G\_A\_0.5$ and G_A_1 are shear modulus on zone A with half and one UCL width. The results indicate that the influence of mesostructure on the macroscopic strain is not high.

The strain range is from 500 to 3000 με for in-plane curves and the moduli are listed in Table 1. Three kinds of moduli are presented according to what macroscopic strain is defined. The results show that the shear modulus defined on line l has a great scatter due to the macroscopic strain is sensitive to the material architecture. With the zone extending, the standard deviation can decrease from 0.51 to 0.25 GPa. As discussed in Sections 3.1 and 3.2, the strain within a unit cell is highly non-uniform and the macroscopic strain strongly depends on the position of the specimen notches. Based on these results, the width of selection zone A is requested one UCL. However, with the width extending, the shear stress may exceed the region of uniform stress and also result in inaccurate reading. In this case, the measurement modulus on zone A may larger than the real modulus, as listed in Table 1, the average modulus increase 3.35–3.85 GPa. The moduli measured by strain-gauge are also listed for comparing. Although the mesoscopic strain is highly non-uniform, the strain-gauge can still give relatively acceptable results when the strain-gauge size is equal to one UCL. But it should be cautious to use strain-gauge measurement. One reason is that the strain-gauge strain is very sensitively to gauge size and position, which is difficult to carry out in experiments. The other is that it is generally needed correction factors when using one point gauge strain as the macroscopic strain of the specimen [58]. However, the correction factors may be difficult to correctly obtain due to the strain distribution.

Table 1
Shear modulus with different macroscopic average strain (GPa).

Specimen	Line l	Zone A		Strain-gauge = 0.5UCL		Strain-gauge = UCL	
		0.5UCL	UCL	Position A	Position B	Position A	Position B
1#	3.55	3.69	4.07	3.68	3.57	4.05	4.01
2#	4.10	4.07	3.59	3.97	3.90	3.48	3.58
3#	2.87	3.24	3.75	3.35	3.03	3.57	3.60
4#	3.31	3.57	4.15	3.48	3.45	3.99	3.97
5#	2.91	3.13	3.67	3.11	2.94	3.59	3.55
Average	3.35	3.54	3.85	3.52	3.38	3.74	3.74
Standard deviation	0.51	0.37	0.25	0.33	0.40	0.26	0.23

4. Conclusions

By using full-field DIC technique, the Iosipescu shear test is carried out for 3D orthogonal woven C/C composites. The mesoscopic strain non-uniformity is clearly observed. Based on present work, several conclusions can be obtained.

(1) The strain is highly non-uniform within one unit cell for in-plane specimens; the degree of strain non-uniformity is not high for through-the-thickness specimens.
(2) The macroscopic strain in the test section strongly depends on the materials structure heterogeneity. For accurate measurement, representative strain average zone should contain one UCL.
(3) If the scale of strain-gauge measurement is equal to one UCL, the strain-gauge can still give relatively acceptable results. However, it should be noted that observed strain measured by the strain-gauge is very sensitive to gauge size and position.

Acknowledgment

Financial support from the National Natural Science Foundation of China (Grant No. 11125210) is gratefully acknowledged.

References

[1] Dow MB, Dexter HB. Development of stitched, braided and woven composite structures in the ACT program and at Langley Research Center. NASA/TP-97-206234; November, 1997.
[2] Huang ZM. The mechanical properties of composites reinforced with woven and braided fabrics. Compos Sci Technol 2000;60(4):479–98.
[3] Tong LY, Tan P, Steven GP, Ishikawa T. Behavior of 3D orthogonal woven CFRP composites. Part I: Experimental investigation. Composites Part A 2000;31(3):259–71.
[4] Mouritz AP, Cox BN. A mechanistic interpretation of the comparative in-plane mechanical properties of 3D woven, stitched and pinned composites. Composites Part A 2010;41(6):709–28.
[5] Subhash G, Walter TR, Sankar BV, Yen CF. Monotonic and cyclic short beam shear response of 3D woven composites. Compos Sci Technol 2010;70(15):2190–7.
[6] Tarnopol'skii YM, Arnautov AK, Kulakov VL. Methods of determination of shear properties of textile composites. Composites Part A 1999;30(7):879–85.
[7] Pagano NJ, Whitney JM. Geometric design of composite cylindrical characterization specimens. J Compos Mater 1970;4:360–78.
[8] Garcia R, Weisshaar TA, Mcwithey RR. An experimental and analytical investigation of the rail shear-test method as applied to composite-materials. Exp Mech 1980;20(8):273–9.
[9] Hussain A, Adams D. The Wyoming-modified two-rail shear test fixture for composite materials. J Compos Technol Res 1999;21(4):215–23.
[10] Adams DF, Hussain AK. Analytical evaluation of the two-rail shear test method for composite materials. Compos Sci Technol 2004;64(2):221–38.
[11] Rosen BW. A simple procedure for experimental determination of longitudinal shear modulus of unidirectional composites. J Compos Mater 1972;6(October):552–4.
[12] Sims DF. In-plane shear stress–strain response of unidirectional composite-materials. J Compos Mater 1973;7(January):124–8.
[13] Odegard G, Kumosa M. Determination of shear strength of unidirectional composite materials with the Iosipescu and 10° off-axis shear tests. Compos Sci Technol 2000;60(16):2917–43.
[14] Walrath DE, Adams DF. The Iosipescu shear test as applied to composite-materials. Exp Mech 1983;23(1):105–10.
[15] Barnes JA, Kumosa M, Hull D. Theoretical and experimental evaluation of the Iosipescu shear test. Compos Sci Technol 1987;28(4):251–68.
[16] Ho H, Tsai MY, Morton J, Farley GL. An experimental investigation of Iosipescu specimen for composite-materials. Exp Mech 1991;31(4):328–36.
[17] Lang EJ, Chou TW. The effect of strain gage size on measurement errors in textile composite materials. Compos Sci Technol 1998;58(3–4):539–48.
[18] Ho H, Tsai MY, Morton J, Farley GL. Inplane shear testing of graphite–woven fabric composites. Exp Mech 1994;34(1):45–52.
[19] Ifju PG, Masters JE, Jackson WC. The use of moire interferometry as an aid to standard test-method development for textile composite-materials. Compos Sci Technol 1995;53(2):155–63.
[20] Masters JE, Ifju PG. A phenomenological study of triaxially braided textile composites loaded in tension. Compos Sci Technol 1996;56(3):347–58.
[21] Hale RD. An experimental investigation into strain distribution in 2D and 3D textile composites. Compos Sci Technol 2003;63(15):2171–85.
[22] Hale RD, Villa M. Influence of opposing wave nesting in compression-loaded composites. J Compos Mater 2003;37(13):1149–66.
[23] Metwalli SM, Ragab AR, Kamel AH, Saheb AA. Determination of plastic stress–strain behavior by digital-image-processing techniques. Exp Mech 1987;27(4):414–22.
[24] Bahlouli N, Guil SM, Ahzi S, Laberge M. Stress–strain response of biomaterials by a digital image correlation method: application to tecoflex. J Mater Sci Technol 2004;20:114–6.
[25] Ukyo S, Masuda M. Investigation of the true stress–strain relation in shear using the digital image correlation method. Mokuzai Gakkaishi 2004;50(3):146–50.
[26] Kamaya M, Kawakubo M. A procedure for determining the true stress–strain curve over a large range of strains using digital image correlation and finite element analysis. Mech Mater 2011;43(5):243–53.
[27] Lambros J, Abanto-Bueno J. Investigation of crack growth in functionally graded materials using digital image correlation. Eng Fract Mech 2002;69(14–16):1695–711.
[28] Roux S, Rethore J, Hild F. Digital image correlation and fracture: an advanced technique for estimating stress intensity factors of 2D and 3D cracks. J Phys D Appl Phys 2009;42(21):214004.
[29] Tippur H, Lee D, Kirugulige M, Bogert P. Experimental study of dynamic crack growth in unidirectional graphite/epoxy composites using digital image correlation method and high-speed photography. J Compos Mater 2009;43(19):2081–108.
[30] Richter-Trummer V, Marques EA, Chaves FJP, Tavares JMRS, da Silva LFM, de Castro PMST. Analysis of crack growth behavior in a double cantilever beam adhesive fracture test by different digital image processing techniques. Materialwiss Werkstofftech 2011;42(5):452–9.
[31] Mogadpalli GP, Parameswaran V. Determination of stress intensity factor for cracks in orthotropic composite materials using digital image correlation. Strain 2008;44(6):446–52.
[32] Du Y, Diaz FA, Burguete RL, Patterson EA. Evaluation using digital image correlation of stress intensity factors in an aerospace panel. Exp Mech 2011;51(1):45–57.
[33] Lyons JS, Liu J, Sutton MA. High-temperature deformation measurements using digital-image correlation. Exp Mech 1996;36(1):64–70.
[34] Grant BMB, Stone HJ, Withers PJ, Preuss M. High-temperature strain field measurement using digital image correlation. J Strain Anal Eng 2009;44(4):263–71.
[35] Pan B, Wu DF, Wang ZY, Xia Y. High-temperature digital image correlation method for full-field deformation measurement at 1200 degrees C. Meas Sci Technol 2011;22(1):015701.
[36] Camanho PP, Koerber H, Xavier J. High strain rate characterisation of unidirectional carbon–epoxy IM7-8552 in transverse compression and in-plane shear using digital image correlation. Mech Mater 2010;42(11):1004–19.
[37] Lord JD, Penn D, Whitehead P. The application of digital image correlation for measuring residual stress by incremental hole drilling. Appl Mech Mater 2008;13–14:65–73.
[38] Korsunsky AM, Sebastiani M, Bemporad E. Residual stress evaluation at the micrometer scale: analysis of thin coatings by FIB milling and digital image correlation. Surf Coat Tech 2010;205(7):2393–403.
[39] Nicoletto G, Anzelotti G, Riva E. Mesoscopic strain fields in woven composites: experiments vs. finite element modeling. Opt Laser Eng 2009;47(3–4):352–9.
[40] Nicoletto G, Anzelotti G, Riva E. Mesomechanic strain analysis of twill-weave composite lamina under unidirectional in-plane tension. Composites Part A 2008;39(8):1294–301.
[41] Ivanov D, Ivanov S, Lomov S, Verpoest I. Strain mapping analysis of textile composites. Opt Laser Eng 2009;47(3–4):360–70.
[42] Yang QD, Rugg KL, Cox BN, Marshall DB. Evaluation of macroscopic and local strains in a three-dimensional woven C/SiC composite. J Am Ceram Soc 2005;88(3):719–25.
[43] Bruck HA, Mcneill SR, Sutton MA, Peters WH. Digital image correlation using Newton–Raphson method of partial–differential correction. Exp Mech 1989;29(3):261–7.
[44] Vendroux G, Knauss WG. Submicron deformation field measurements. Part 1: Developing a digital scanning tunneling microscope. Exp Mech 1998;38(1):18–23.
[45] Vendroux G, Knauss WG. Submicron deformation field measurements. Part 2: Improved digital image correlation. Exp Mech 1998;38(2):86–92.
[46] Zhou P, Goodson KE. Subpixel displacement and deformation gradient measurement using digital image/speckle correlation (DISC). Opt Eng 2001;40(8):1613–20.
[47] Pan B, Qian KM, Xie HM, Asundi A. Two-dimensional digital image correlation for in-plane displacement and strain measurement: a review. Meas Sci Technol 2009;20(6):1–17.
[48] Lee S, Munro M. Evaluation of testing techniques for the Iosipescu shear test for advanced composite-materials. J Compos Mater 1990;24(4):419–40.
[49] Siron O, Pailhes J, Lamon J. Modelling of the stress/strain behaviour of a carbon/carbon composite with a 2.5 dimensional fibre architecture under tensile and shear loads at room temperature. Compos Sci Technol 1999;59(1):1–12.
[50] Kumosa M, Odegard G, Armentrout D, Kumosa L, Searles K, Sutter JK. Comparison of the +/−45° Iosipescu shear tests for woven fabric composite materials. J Compos Technol Res 2002;24(1):3–16.
[51] Gentz M, Armentrout D, Rupnowski P, Kumosa L, Sutter JK, Kumosa M. Mechanical behavior of a woven graphite/PMR-15 composite at room and elevated temperatures determined from the +/−45° tensile and Iosipescu shear tests. J Compos Technol Res 2003;25(1):22–34.
[52] Rupnowski P, Gentz M, Sutter JK, Kumosa M. Mechanical response of a woven graphite/polyimide composite to in-plane shear dominated loads at room and elevated temperatures. Acta Mater 2004;52(19):5603–13.
[53] Gentz M, Armentrout D, Rupnowski P, Kumosa L, Shin E, Sutter JK, et al. In-plane shear testing of medium and high modulus woven graphite fiber reinforced/polyimide composites. Compos Sci Technol 2004;64(2):203–20.
[54] Walrath DE, Adams DF. The Iosipescu shear test as applied to composite-materials. Exp Mech 1983;23(1):105–10.
[55] Conant NR, Odom EM. An improved Iosipescu sheer test fixture. J Compos Technol Res 1995;17(1):50–5.
[56] Searles K, Odegard G, Kumosa M. The effect of eccentric loads on the macroscopic strain and stress distributions in woven fabric composite Iosipescu specimens. J Compos Mater 2002;36(5):571–88.
[57] Yoneyama S, Kikuta H, Kitagawa A, Kitamura K. Lens distortion correction for digital image correlation by measuring rigid body displacement. Opt Eng 2006;45(2):023602.
[58] Ho H, Tsai MY, Morton J, Farley GL. Numerical-analysis of the Iosipescu specimen for composite-materials. Compos Sci Technol 1993;46(2):115–28.